Available online at www.sciencedirect.com
SCIENCE DIRECT®
Optics Communications 216 (2003) 247–260
OPTICS COMMUNICATIONS
www.elsevier.com/locate/optcom

Diffraction theory of imaging with X-ray compound refractive lens

V. Kohn [a], I. Snigireva [b], A. Snigirev [b,*]

[a] *Russian Research Centre "Kurchatov Institute", 123182 Moscow, Russia*
[b] *European Synchrotron Radiation Facility, BP220, F-38043 Grenoble, France*

Received 12 April 2002; received in revised form 2 August 2002; accepted 21 November 2002

Abstract

Specific features of X-ray compound refractive lens (XCRL) with parabolic profile of concave surfaces for hard X-ray focusing and micro-imaging are analyzed theoretically. Large longitudinal size L of the XCRL requires a verification of the thin lens approximation widely used in the literature. We show that the parabolic XCRL can be treated as a thin lens placed in the middle of the XCRL with the focal length $F_1 = F + L/6$, where F is the XCRL focal distance in the thin lens approximation. The relatively small aperture of XCRL due to the absorption of X-rays leads to finite resolution and phase effects (or artifacts) of the images. This feature reveals itself as a visibility of transparent objects. It is shown that XCRL allows one to visualize the local phase gradient of the radiation wave field produced by the object. This opens quite a new technique of micro-imaging for purely phase objects which is different from the traditional phase contrast micro-imaging techniques. Optical properties of XCRL as a Fourier transformer are considered as well.

Keywords: Hard X-rays; Focusing; Microimaging; Compound refractive lens; Synchrotron radiation; Lens aperture; Lens focal distance

1. Introduction

Since the first successful demonstration [1] of X-ray compound refractive lens (XCRL) for focusing a synchrotron radiation beam delivered by the third generation sources, the X-ray refractive optics is under extensive development. In addition to aluminium [2–9], different low-Z materials: beryllium [2,5,7,9], silicon [10–12], organic compounds [2,5,13–18] were experimentally tested. The lens with cylindrical holes drilled in cross geometry allows two-plane focusing [2–4,15]. The interesting solution is the planar refractive lens with the parabolic profile which can be either single or compound [10–12]. Of course, the lens with parabolic profile and rotational symmetry around the optical axis has a lot of advantages for the two-plane focusing and micro-imaging [6,8,9]. There are successful attempts to develop the refractive optics by means of various approaches [19–24]. Significant

* Corresponding author. Fax: +33-4-76-88-2542.
E-mail address: snigirev@esrf.fr (A. Snigirev).

0030-4018/02/$ - see front matter
doi:10.1016/S0030-4018(02)02285-X

contributions in the XCRL theory are made in [1,3,8,25–27].

Unlike visible light optics, X-ray collecting lens has a concave shape and the material of the lens is always absorbing. This leads to a significant limitation of the XCRL effective aperture a_γ even though the physical transverse size a of the lens can be much larger. The XCRL has a rather large longitudinal size L so that the thin lens approximation must be verified. We treat L as the XCRL length. Compared to the visible light lens, the ratio a_γ/L for the XCRL is very small. This property influences the operation of XCRL as an imaging device. When the ratio a_γ/L is extremely small, it can be shown that the phenomenon like the X-ray beam channeling occurs. However, in most practical cases XCRL satisfies the condition $L/F \ll 1$ where F is the XCRL focal length in the thin lens approximation. Therefore it is sufficient to consider only the linear corrections in L/F beyond the thin lens approximation.

In this work we present the diffraction theory of a parabolic XCRL. We explain the experimentally observed phase-contrast artifacts in imaging transparent objects which becomes visible even in the image plane of the XCRL for which the lens formula is fulfilled [28,29]. These images show up as edge enhanced images where the boundaries and interfaces of the object generate both bright and dark contrast. These features cannot be explained within the geometrical optics approximation, and they are pure diffraction phenomena.

The paper is organized as follows. Section 2 presents the detailed theory of the one-dimensional parabolic XCRL. We formulate the theory in terms of the propagators, calculate the XCRL propagator in first-order L/F approximation, and obtain the total image propagator in the analytical form. We found that the parabolic XCRL can be treated as a thin lens, placed in the middle of the XCRL, with the focal length $F_1 = F + L/6$. We also discuss properties of the quasi-Fourier image at the back focal plane (distance equal to the XCRL focal length) and the quasi-focused image at the image plane (distance satisfying the lens formula). The computer simulations allow us to confirm the derived analytical formulas. In Section 3 we consider the problem of 2D imaging applying the results, obtained in the Section 2. We show that the XCRL two-dimensional propagator is a product of one-dimensional propagators. This property allows one to simplify the problem in many practicable cases.

2. The diffraction theory of the 1-D imaging with parabolic X-ray compound refractive lenses

For the sake of simplicity, we consider first a one-dimensional case of an in-line setup where the object and the parabolic XCRL are homogeneous along the y-axis. Under these conditions, the recorded image or intensity distribution is homogeneous along the y-axis. Therefore we can omit the calculation of the integrals over the y coordinate.

2.1. The formulation of the image problem via propagators

We assume the optical axis to be coincide with the z-axis of the coordinate system (see Fig. 1). The x-dependence behind the object of the complex X-ray wave field, including also the incident wave, is described by the complex function $A_o(x_o)$ which hereafter is called the object wave field. We will neglect the longitudinal size of the object compared to the other distances of our setup. The XCRL with the parabolic profile of individual components is located at the distance r_o from the object. The XCRL has a length L so that the distance r_o is assumed to be between the object and the front side of the XCRL.

It is easy to write the x-dependence of the complex wave field $A_f(x_f)$ in front of the XCRL in terms of the paraxial approximation to the Kirchhoff integral [30]

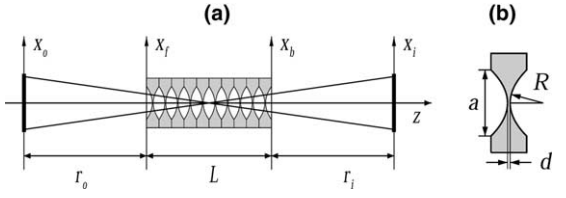

Fig. 1. Geometrical parameters of the experimental setup (a) and of the individual lens in the XCRL array (b).

$$A_{\mathrm{f}}(x_{\mathrm{f}}) = \int \mathrm{d}x_{\mathrm{o}} P(x_{\mathrm{f}} - x_{\mathrm{o}}, r_{\mathrm{o}}) A_{\mathrm{o}}(x_{\mathrm{o}}). \quad (1)$$

Here the coordinate x_{f} is related to the axis in front of the XCRL and $P(x,z)$ is the propagator for the transversal x-dependence of the field through the free space along the z-axis

$$P(x,z) = \frac{1}{(\mathrm{i}\lambda z)^{1/2}} \exp\left(\mathrm{i}\pi \frac{x^2}{\lambda z}\right), \quad (2)$$

where λ is a wavelength of the monochromatic wave. Hereafter we imply that the limits of integrals are infinite if the opposite is not specified.

The next step is to calculate the x-dependence of the complex wave field behind the XCRL. Let us represent the solution of this task through the propagator of the XCRL in the form

$$A_{\mathrm{b}}(x_{\mathrm{b}}) = \int \mathrm{d}x_{\mathrm{f}} P_{\mathrm{l}}(x_{\mathrm{b}}, x_{\mathrm{f}}; L) A_{\mathrm{f}}(x_{\mathrm{f}}), \quad (3)$$

where x_{b} is the coordinate in the direction normal to the axis z behind the XCRL (see Fig. 1). The complex wave field $A_{\mathrm{i}}(x_{\mathrm{i}})$ at the image axis, which is placed at the distance r_{i} from the back side of the XCRL, can be expressed through the Kirchhoff integral once again

$$A_{\mathrm{i}}(x_{\mathrm{i}}) = \int \mathrm{d}x_{\mathrm{b}} P(x_{\mathrm{i}} - x_{\mathrm{b}}, r_{\mathrm{i}}) A_{\mathrm{b}}(x_{\mathrm{b}}). \quad (4)$$

Substituting (1) and (3) into (4) and changing the order of integration, we obtain the relation between the object wave field $A_{\mathrm{o}}(x_{\mathrm{o}})$ and the image wave field $A_{\mathrm{i}}(x_{\mathrm{i}})$ in terms of the image propagator $G(x_{\mathrm{i}}, x_{\mathrm{o}})$ as follows:

$$A_{\mathrm{i}}(x_{\mathrm{i}}) = \int \mathrm{d}x_{\mathrm{o}} G(x_{\mathrm{i}}, x_{\mathrm{o}}) A_{\mathrm{o}}(x_{\mathrm{o}}), \quad (5)$$

where

$$G(x_{\mathrm{i}}, x_{\mathrm{o}}) = \int \mathrm{d}x_{\mathrm{b}} P(x_{\mathrm{i}} - x_{\mathrm{b}}, r_{\mathrm{i}}) \times \int \mathrm{d}x_{\mathrm{f}} P_{\mathrm{l}}(x_{\mathrm{b}}, x_{\mathrm{f}}; L) P(x_{\mathrm{f}} - x_{\mathrm{o}}, r_{\mathrm{o}}). \quad (6)$$

In order to calculate the integral, we need to specify the explicit form of the XCRL propagator $P_{\mathrm{l}}(x_{\mathrm{b}}, x_{\mathrm{f}}; L)$.

We note any solution of the Maxwell's equation must satisfy the reciprocity principle, i.e., the replacement x_{i} by x_{o} and simultaneously r_{i} by r_{o} and vice versa must lead to the same result. Expression (6) satisfies this principle if the XCRL propagator is a symmetrical function of variables x_{b} and x_{f}.

2.2. The X-ray compound refractive lens propagator

So far the thin lens approximation, i.e., the zero-order approximation in parameter L/F was assumed in the theory of imaging with XCRL. Violation of this approximation in the specific case of focusing the parallel beam was analyzed only within the frame of the geometrical optics [19,25]. In the paraxial approximation the focal length $F = R/2N\delta$ [1], where R is the radius of curvature of the parabolic profile (near the vertex), N is the total number of the individual parabolic lenses (see Fig. 1 where $N = 10$), δ is the decrement of the complex refractive index $n = 1 - \delta + \mathrm{i}\beta = 1 - \eta$ of the lens material. The XCRL propagator in this case has a form [3]

$$P_{\mathrm{l}}(x_{\mathrm{b}}, x_{\mathrm{f}}; L) = \exp[-\mathrm{i}k\eta t(x_{\mathrm{b}})]\delta(x_{\mathrm{b}} - x_{\mathrm{f}}). \quad (7)$$

Hereafter $k = 2\pi/\lambda$ is the wave-number, $\delta(x)$ is the Dirac delta-function, and $t(x)$ is the variable thickness of XCRL material along the optical axis. For the XCRL with a parabolic profile

$$t(x) = N\left[\frac{x^2}{R} + d\right], \quad |x| < \frac{a}{2}, \quad L = t\left(\frac{a}{2}\right). \quad (8)$$

Here d is the minimum spacing between two parabolas, L is the XCRL length, and a is the XCRL geometrical transverse size. Assuming that a is larger than the effective aperture $a_\gamma = (\lambda F/\gamma)^{1/2}$ where $\gamma = \beta/\delta$, we can neglect the geometrical aperture of the XCRL. This expression for the propagator corresponds to the local approximation, i.e., at each x point the wave field is multiplied by an exponential factor known as a transmission function.

We want to obtain the XCRL propagator in the first-order approximation, i.e., to take into account the corrections linear in L/F. The compound lens consists of N closely packed identical individual lenses. Taking this into account we can consider XCRL as a periodic structure of N elements with the period L/N. If N is large each simple lens makes slight perturbation of the wave field. Under these conditions we can use the

continuous approximation [3] which is obtained after averaging the density of XCRL matter over the period along the optical axis. Then the Maxwell's wave equation inside the XCRL takes the form:

$$\left[\frac{\mathrm{d}^2}{\mathrm{d}z^2}+\frac{\mathrm{d}^2}{\mathrm{d}x^2}+k^2n^2(x)\right]E(x,z)=0, \tag{9}$$

where $E(x,z)=\exp(\mathrm{i}kz)A(x,z)$ in the paraxial approximation and $n(x)=1-\eta(x)$ with

$$\eta(x)=\frac{c}{L}\left[\frac{x^2}{2F}+\delta dN\right],\quad c=1-\mathrm{i}\gamma,\quad \gamma=\frac{\beta}{\delta}. \tag{10}$$

This expression is valid only inside the geometrical aperture of the XCRL $|x|<a/2$. Since we assume that the geometrical aperture a exceeds the effective aperture a_γ, the region $|x|>a/2$ represents no interest. Taking into account that $|\eta(x)|\ll 1$ and applying the paraxial approximation we obtain from (9) the parabolic equation for the slowly varying part of the field $A(x,z)$ as follows:

$$\frac{\mathrm{d}A}{\mathrm{d}z}=-\mathrm{i}k\eta(x)A+\frac{\mathrm{i}}{2k}\frac{\mathrm{d}^2A}{\mathrm{d}x^2}. \tag{11}$$

This equation must be solved inside the interval $0<z<L$ with the boundary condition $A(x,0)=A_\mathrm{f}(x)$. We are interested in the function $A_\mathrm{b}(x)=A(x,L)$.

One can see that the transmission function $\exp(-\mathrm{i}k\eta(x)z)$ corresponding to (7) is a solution of this equation if the second term on the right-hand-side of (11) is negligible. On the other hand, the propagator (2) is the solution of (11) with $\eta(x)=0$, i.e., in a free space. We try the approximate solution of (11) in the form

$$A(x,z)=A_\mathrm{o}(x,z)\exp[-\mathrm{i}kf(x,z)], \tag{12}$$

where

$$A_\mathrm{o}(x,z)=\int \mathrm{d}x_\mathrm{f}P(x-x_\mathrm{f},z)A_\mathrm{f}(x_\mathrm{f}),\qquad \frac{\mathrm{d}A_\mathrm{o}}{\mathrm{d}z}=\frac{\mathrm{i}}{2k}\frac{\mathrm{d}^2A_\mathrm{o}}{\mathrm{d}x^2} \tag{13}$$

and $f(x,z)$ is new unknown function.

Substituting (12) in (11) and taking into account (13), we obtain the equation for $f(x,z)$ as

$$\frac{\mathrm{d}f}{\mathrm{d}z}=\eta(x)-\alpha(x,z)\frac{\mathrm{d}f}{\mathrm{d}x}+\frac{1}{2}\left(\frac{\mathrm{d}f}{\mathrm{d}x}\right)^2+\frac{\mathrm{i}}{2k}\frac{\mathrm{d}^2f}{\mathrm{d}x^2} \tag{14}$$

with the boundary condition $f(x,0)=0$. Here

$$\alpha(x,z)=\frac{1}{\mathrm{i}kA_\mathrm{o}(x,z)}\frac{\mathrm{d}A_\mathrm{o}(x,z)}{\mathrm{d}x} \tag{15}$$

is the known function which slowly varies with z. When $L/F\ll 1$, we can neglect the z-dependence in $\alpha(x,z)$ and take $\alpha(x)$ at $z=0$. Then replacing A_o by A_f and taking into account (1), we have

$$\alpha(x)=\frac{[x-\bar{x}_\mathrm{o}(x)]}{r_\mathrm{o}},\qquad \bar{x}_\mathrm{o}(x)=\frac{\int \mathrm{d}x'P(x-x',r_\mathrm{o})x'A_\mathrm{o}(x')}{\int \mathrm{d}x'P(x-x',r_\mathrm{o})A_\mathrm{o}(x')}. \tag{16}$$

We see that the average coordinate of an object $\bar{x}_\mathrm{o}(x)$ has a rather complicated structure and does not allow us to formulate the solution of the problem in terms of linear propagator like the free space propagator. We want to use the same approximation as in [3] and replace $\bar{x}_\mathrm{o}(x)$ by x_o. This approximation is well suited for the XCRL use as an imaging device. Then $\alpha(x)=(x-x_\mathrm{o})/r_\mathrm{o}$.

The approximate solution for $f(x,L)$ is derived by iterations (see [3]). For the zero approximation we neglect the transverse derivatives in (14) and obtain $f_\mathrm{o}(x,z)=\eta(x)z$. The first approximation $f_1(x,L)=f_1(x_\mathrm{b},x_\mathrm{o})$ is obtained by substitution the transverse derivatives of $f_\mathrm{o}(x,z)$ instead of $f(x,z)$ in the right-hand-side of (14). As a result we obtain

$$f(x,L)=\eta L-\frac{L^2}{2}\frac{(x-x_\mathrm{o})}{r_\mathrm{o}}\frac{\mathrm{d}\eta}{\mathrm{d}x}+\frac{L^3}{6}\left(\frac{\mathrm{d}\eta}{\mathrm{d}x}\right)^2+\frac{\mathrm{i}L^2}{4k}\frac{\mathrm{d}^2\eta}{\mathrm{d}x^2}. \tag{17}$$

Thus we obtain the propagator of a XCRL in the next approximation in L/F as

$$P_1(x_\mathrm{b},x_\mathrm{f};L)=\exp[-\mathrm{i}kf_1(x_\mathrm{b},x_\mathrm{o})]P(x_\mathrm{b}-x_\mathrm{f},L). \tag{18}$$

As a result, for the image propagator (6) we have

$$G(x_\mathrm{i},x_\mathrm{o})=\int \mathrm{d}x_\mathrm{b}P(x_\mathrm{i}-x_\mathrm{b},r_\mathrm{i})\exp[-\mathrm{i}kf_1(x_\mathrm{b},x_\mathrm{o})]\times P(x_\mathrm{b}-x_\mathrm{o},r_\mathrm{o}+L). \tag{19}$$

Here we applied the well-known property of the free-space propagator (see discussion in [31]) that the convolution of two propagators is again the propagator for the total distance, namely, $P(x_1-x,z_1)\ *\ P(x-x_2,z_2)=P(x_1-x_2,z_1+z_2)$.

We note the solution (19) does not satisfy straightforwardly the reciprocity principle. In principle, more accurate solution that satisfies the reciprocity principle can be obtained. However, the derivation is more complicated and the difference involves higher orders in small parameter L/F. We will solve this problem later on at least for the case of imaging.

2.3. Analytical solution for the image propagator

In this section we obtain an analytical expression for integral (19). Taking into account (2), (10) and (17), we write

$$G(x_i,x_o)=\frac{C_0}{i\lambda(r_o r_i)^{1/2}}\int dx_b \exp\left(i\frac{k}{2}\varphi(x_i,x_b,x_o)\right), \tag{20}$$

where

$$\begin{aligned} C_0&=\exp\left[c\left(-ik\delta dN+\frac{L}{4F}\right)\right],\\ \varphi&=\varphi_0+\varphi_1=U-Vx_b+Wx_b^2,\\ \varphi_0&=\frac{[x_i-x_b]^2}{r_i}+\frac{[x_b-x_o]^2}{r_o}-c\frac{x_b^2}{F},\\ \varphi_1&=-L\left(\frac{[x_b-x_o]^2}{r_o^2}+\frac{x_b^2}{3F^2}-\frac{x_b(x_b-x_o)}{r_o F}\right). \end{aligned} \tag{21}$$

Hereafter we take into account that our accuracy does not exceed first order in L/F. We assume that the parameter γ is of the same order of smallness as L/F or less. A correction from the distance L in the pre-exponential factor does not influence the transverse distribution of the wave field, i.e., the object image.

The parameters $U=U_0+U_1$, $V=V_0+V_1$ and $W=W_0+W_1$ contain the terms of zero and first order in L/F. To satisfy the reciprocity principle in U_1, V_1 and W_1, we apply the relations between x_o, r_o, x_i, r_i and F, resulting from the conditions $V_0=0$ and $W_0=0$ which correspond to the thin lens formula in zero approximation. This is possible, at least for the imaging problem, because the difference is only due to the terms of higher order in L/F. This way we obtain the expressions for U, V and W in terms of the modified distances

$$r_{ol}=r_o+\frac{L}{2},\quad r_{il}=r_i+\frac{L}{2},\quad F_l=F+\frac{L}{6} \tag{22}$$

as follows:

$$\begin{aligned} U&=\frac{x_o^2}{r_{ol}}+\frac{x_i^2}{r_{il}},\quad V=2\left(\frac{x_o}{r_{ol}}+\frac{x_i}{r_{il}}\right),\\ W&=-\frac{c}{F_l}+\frac{1}{r_{ol}}+\frac{1}{r_{il}}. \end{aligned} \tag{23}$$

Now one can see that all the expressions (23) are symmetrical with respect to the permutation of the object and the image. New distances are measured from the middle of the XCRL. The focal length of XCRL increases by $L/6$ compared to the thin lens approximation. New magnitude of the focal length of a XCRL is the main result of our approach. This result was already obtained [3], but in the implicit form.

Applying the table integral, we arrive at the analytical expression in the form

$$G(x_i,x_o)=\frac{C_0}{(i\lambda r_g)^{1/2}}\exp\left(i\frac{\pi}{\lambda r_g}\left[g_i x_i^2-2x_i x_o+g_o x_o^2\right]\right), \tag{24}$$

where

$$\begin{aligned} r_g&=r_{il}+r_{ol}-c\frac{r_{il}r_{ol}}{F_l},\quad g_i=1-c\frac{r_{ol}}{F_l},\\ g_o&=1-c\frac{r_{il}}{F_l}. \end{aligned} \tag{25}$$

The analytical solution allows us to analyze the peculiarities of the XCRL operation in the specific cases and to clarify the difference between the X-ray optics and the visible optics. Notice that the image propagator $G(x_i,x_o)$ coincides with the free-space one (2) $P(x_i-x_o,r_{il}+r_{ol})$ if $F_l=\infty$ and $C_0=1$.

2.4. Quasi-Fourier image

Let us consider the complex coherent wave field at the plane right after the object. This might be a transmission function of the object illuminated by a plane wave or a product of the transmission function and the wave field created by the point source or any other wave field resulting from diffraction by other objects upstream. As is known from the theory of classical refractive optics [30], the complex wave field is converted into its Fourier

transform in the back focal plane of the lens. The distance before the lens does not influence the modulus, but leads to the additional phase factor which vanishes when the object is located in the front focal plane. This property is valid approximately for a XCRL as well. As follows from (5) and (25), the real part of the complex coefficient g_o vanishes when the condition $r_{il} = F_l$ or $r_i = F - L/3$ is fulfilled.

Thus we conclude once again that the real focal length of a XCRL is larger compared to the thin lens limit by $L/6$, when it is counted from the middle of the XRCL. Under this condition we have

$$A_i(x_i) = \frac{C_0 C_l(x_i) C_f(x_i)}{(i\lambda r_f)^{1/2}} \times \int dx_o \exp(-iqx_o - \varepsilon x_o^2) A_o(x_o), \tag{26}$$

where

$$C_f(x) = \exp\left(i\pi \frac{x^2}{\lambda F_l}\right),$$
$$C_l(x_i) = \exp\left(-i\pi \frac{x_i^2}{\lambda F_l} \frac{r_{ol}}{r_f}\right), \tag{27}$$
$$q = \frac{2\pi x_i}{\lambda r_f}, \quad \varepsilon = \frac{\pi}{\lambda}\frac{\gamma}{r_f}, \quad r_f = F_l + i\gamma r_{ol}.$$

The parameter r_f is a complex magnitude. Its real part equals F_l whereas the imaginary part is proportional to r_{ol}.

The known result of the classical optics follows from the formulas (26), (27) in the case of infinite aperture and $\gamma = 0$. However, the XCRL is always absorbing and this leads to the fact that the XCRL reproduces the Fourier image of the modified object function

$$\tilde{A}_o(x_o) = A_o(x_o) \exp\left(-\frac{\pi}{\lambda}\frac{\gamma}{r_f} x_o^2\right). \tag{28}$$

The modification is more stronger the larger the parameter γ is.

Another feature of XCRL is that, in general case, the intensity distribution of the diffraction pattern in the transform plane depends on the object distance r_o due to absorption of X-rays inside the XCRL. This is in contrast to classical optics, where lenses with large aperture are treated and the modulus of the Fourier image is independent of the wave field plane. This property is verified by (26), (27). When $\gamma = 0$, the parameter r_f coincides with F_l. In the case of XCRL, where $\gamma > 0$, the Fourier image is conditional because the wave-number parameter q becomes complex. The imaginary part of q can be decreased by placing the object just in front of the XCRL when $r_o = 0$. We note the factor $|C_l(x_i)|^2$ becomes also position sensitive if $\gamma > 0$.

Let us discuss the quasi-Fourier image in two simple examples. In the first example the object radiates the plane wave $\exp(ikz)$, i.e., $A_o(x_o) = A_o = \text{const}$. The calculation of the integral (26) is straightforward and we obtain

$$A_i(x_i) = A_o \frac{C_0 C_f(x_i)}{(i\gamma)^{1/2}} \exp\left(-\frac{\pi}{\lambda}\frac{x_i^2}{\gamma F_l}\right) \tag{29}$$

and for the integral intensity

$$\bar{I}_l = \int dx_i |A_i(x_i)|^2 = \left(\frac{\lambda F_l}{2\gamma}\right)^{1/2} |A_o C_0|^2. \tag{30}$$

It is of interest to compare these formulas with the case of a thin transparent lens of finite aperture a.

The result can be obtained from (26) with $C_0 = 1$, $\gamma = 0$, $L = 0$, $A_o(x) = A_o\theta(a/2 - x)$. Here $\theta(x)$ is the step function which equals unity for $x > 0$ and zero for $x < 0$. We have

$$A_{it}(x_i) = A_o\left(\frac{\lambda F}{i}\right)^{1/2} \frac{C_l(x_i) C_f(x_i)}{\pi x_i} \times \sin\left(\frac{a\pi}{\lambda F} x_i\right), \tag{31}$$
$$\bar{I}_{it} = a|A_o|^2.$$

According to (29) the intensity $I_i(x_i) = |A_i|^2$ depends on the coordinate x_i as the Gaussian with the FWHM $\sigma_\gamma = 0.664(\lambda F\gamma)^{1/2}$ independent of r_o.

Let us compare this value with the diffraction limited resolution σ_a of the thin transparent lens limited by an aperture a taken from (31), namely, $\sigma_a = 0.886\lambda F/a$. One can determine the effective aperture of the XCRL via the condition $\sigma_\gamma = \sigma_a$. This leads to the result $a_\gamma^{(1)} = 1.334(\lambda F/\gamma)^{1/2}$. Another way is to use the fact that the normalized intensity, integrated within the focal spot, is equal to the aperture for the transparent lens. Then from (30) we obtain $a_\gamma^{(2)} = 0.707(\lambda F/\gamma)^{1/2}$. This is approximately twice as less than the preceding

determination. Thus there is some difference between the transparent lens of the finite aperture and the absorbing parabolic lens.

It is a good choice to use the intermediate value

$$a_\gamma = \left(\frac{\lambda F_l}{\gamma}\right)^{1/2} \approx 2.51\left(\frac{R}{\mu N}\right)^{1/2} \tag{32}$$

for the aperture of the XCRL. In the second expression of (32) we replaced F by $R/2N\delta$ and took into account the linear absorption coefficient $\mu = 4\pi\beta/\lambda$. In case of using the numerical aperture $\text{N.A.} = 2(\delta/\mu F)^{1/2}$ (see, i.e., [16]) we see that $\text{N.A.} = 1.77a_\gamma/F = 1.18\lambda/\sigma_\gamma$. We note the resolution $\sigma_\gamma \to 0$ when $R \to 0$. This fact was used in [32] for a justification of micro-ball refractive optics. However, in this case the aperture and the integral intensity are close to zero even for parabolic shape of micro-lens. For the spherical micro-ball lens, the aperture is smaller due to the inappropriate shape.

In the second example the object is very narrow slit, i.e., $A_o(x_o) = A_o\delta(x_o - x_S)$. The calculation is straightforward again and we obtain

$$A_i(x_i) = A_o \frac{C_0 C_f(x_i)}{(i\lambda r_f)^{1/2}} \exp\left(-i\pi \frac{x_i}{\lambda r_f}\left[x_i \frac{r_{ol}}{F_l} + 2x_S\right]\right) \times \exp\left(-\frac{\pi\gamma}{\lambda r_f} x_S^2\right). \tag{33}$$

Now the intensity $I_i = |A_i|^2$ evidently depends on r_o. If $r_{ol} \approx 0$, $r_f \approx F_l$ the intensity does not depend on the coordinate x_i, i.e., it behaves like Fourier image. However, its magnitude is modified by absorption in the XCRL, and only the slit at the position $|x_S| < a_\gamma/2$ can be detected. As the distance r_o increases, the intensity distribution shows more and more complicated picture. In the limiting case of very long distance when $\gamma r_{ol} \gg F_l$, we can replace r_f by the imaginary value $i\gamma r_{ol}$. Now the intensity distribution considerably differs from the Fourier image of the narrow slit

$$A_i(x_i) = A_o \frac{C_0 C_f(x_i)}{i(\lambda\gamma r_{ol})^{1/2}} \exp\left(-\frac{\pi}{\lambda}\frac{[x_i - x_{is}]^2}{\gamma F_l}\right) \times \exp\left(\frac{\pi x_S^2}{\lambda r_{ol}}\left[i + \frac{F_l}{\gamma r_{ol}}\right]\right). \tag{34}$$

Here $x_{is} = -x_S F_l/r_{ol}$. As follows from this expression, the intensity distribution has a maximum value at the point x_{is}. The corresponding peak is symmetrical and has the same width as in the case of the plane wave considered above.

We conclude that the XCRL always transforms the wave field distribution in front of the finite aperture of the XCRL. The resolution of the transformation is limited by the diffraction phenomena due to the finite aperture. In the last example, the small object far removed from the XCRL produces approximately the plane wave in front of the XCRL, and instead of the Fourier image focusing will occur.

2.5. Quasi-focused image

Let us consider the image formation with the XCRL when the lens formula

$$\frac{1}{r_{il}} + \frac{1}{r_{ol}} - \frac{1}{F_l} = 0 \tag{35}$$

is fulfilled. In this case the real part of r_g vanishes and the XCRL propagator (24) can be written in the form

$$G(x_i, x_o) = \frac{C_0}{i}\left(\frac{r_{ol}}{r_{il}}\right)^{1/2} \exp\left(i\frac{\pi}{\lambda}\left[\frac{x_i^2}{r_{il}} + \frac{x_o^2}{r_{ol}}\right]\right) \times \delta_\sigma(x_o - x_{oi}), \tag{36}$$

where

$$\delta_\sigma(x) = \frac{1}{\sigma(2\pi)^{1/2}} \exp\left(-\frac{x^2}{2\sigma^2}\right), \quad \sigma = \frac{\lambda r_{ol}}{a_\gamma(2\pi)^{1/2}}, \quad x_{oi} = -x_i\frac{r_{ol}}{r_{il}}. \tag{37}$$

We note $\delta_\sigma(x)$ becomes the Dirac delta-function $\delta(x)$ in the limit $\sigma \to 0$.

For the transparent lens of the infinite aperture, we have $\gamma = 0$. Replacing $\delta_\sigma(x)$ by $\delta(x)$, we obtain from (5) the simple relation between the object function $A_o(x_o)$ and the image function $A_i(x_i)$ as

$$A_i(x_i) = \frac{C_0}{i}\left(\frac{r_{ol}}{r_{il}}\right)^{1/2} C_i(x_i) A_o(x_{oi}), \quad C_i(x) = \exp\left(i\pi\frac{x^2}{\lambda F_l}\frac{r_{ol}}{r_{il}}\right). \tag{38}$$

Thus, the wave field measured in the image plane is proportional to the wave field in the object plane,

taking into account the magnification factor, i.e., the ratio between r_{il} and r_{ol}. An additional phase factor in the propagator does not influence the intensity in this case. An opaque (absorbing) object will produce the direct image, whether the transparent (non-absorbing) object remains invisible, although the phase profile after the object is modified.

As we mentioned, in reality, the XCRL has a finite aperture a_γ and a finite resolution σ because $\gamma > 0$. Therefore, if the transparent object produces a drastic perturbation of the phase profile of the incident wave field with the characteristic length less than σ, it can be detectable in the image plane. We note the resolution σ is proportional to the distance r_{ol}. However, contrary to Fourier imaging, we have no possibility to decrease the distance r_{ol} because it cannot be less than F_l due to the lens formula.

Under coherent illumination with the quasi-parallel beam the XCRL makes visible only the finite region of the object. To show this we calculate a quasi-image in the case where the wave field behind the object is the plane wave directed along the optical axis, i.e., $A_o(x_o) = 1$. The integral (5) for this case has the analytical expression as $A_i(x_i) = Q(x_i)$ where

$$Q(x_i) = \frac{C_0}{i}\left(\frac{r_{ol}}{r_{il}p}\right)^{1/2} C_i(x_i)\exp\left(-\frac{\pi}{p}\frac{x_{oi}^2}{a_\gamma^2}\right), \qquad p = 1 - i\gamma\frac{r_{ol}}{F_l}. \tag{39}$$

Here a_γ is determined by (32). When $\gamma r_{ol} \gg F_l$ we arrive at the result (29) again. The point is that $r_{il} \approx F_l$ in this case, according to the lens formula (35) and because $\gamma \ll 1$. For more practicable case when $\gamma r_{ol} \ll F_l$, we obtain the intensity varying as

$$I_{ib}(x_i) \approx \frac{r_{ol}}{r_{il}}\exp\left(-2\pi\frac{x_{oi}^2}{a_\gamma^2}\right). \tag{40}$$

The FWHM of the intensity distribution, is independent of distances and equal to $a_{ov} = 0.664a_\gamma$ in terms of the corresponding coordinate at the object x_{oi}. The physical reason of this phenomenon lies in the fact that the image propagator (36) in addition to the finite resolution contains the phase factor $\exp[i\varphi(x_o)]$ with $\varphi = \pi x_o^2/\lambda r_{ol}$ modifying the object wave field. For the given value of x_i, the effective region of integration is $x_{oi} - \sigma < x_o < x_{oi} + \sigma$. The speed of the phase change inside this region can be estimated as $d\varphi/dx_o = 2\pi|x_i|/\lambda r_{il}$, whereas the total phase shift within the region is $\Delta\varphi = 2\sigma(d\varphi/dx_o) = (2\pi)^{1/2}|x_{oi}|/a_\gamma$. Substituting $|x_{oi}| = a_{ov}/2$, we obtain that the intensity decreases twice when $\Delta\varphi = 0.83 \approx \pi/4$.

Let us discuss the possible cases of visibility of a transparent object. We consider first a simple object which may be called the "phase step". It produces the phase shift $\exp(i\psi)$ in the region $x_S < x_o < \infty$. In this case one has to calculated the integral (5) with $A_o(x_o) = 1 + [\exp(i\psi) - 1]\,\theta(x_o - x_S)$. The first term (unity) leads to expression (39) where the value of complex Fresnel integral with infinite upper limit is used. The second term leads to expression involving the complex Fresnel integral

$$F_\Phi(Z) = \int_0^Z \exp\left(i\frac{\pi}{2}t^2\right)dt, \qquad F_\Phi(-Z) = -F_\Phi(Z) \tag{41}$$

with the finite upper limit. Taking this into account and calculating the accurate value of the upper limit one arrives to the accurate solution which may be written as follows:

$$A_i(x_i) = \frac{1}{2}Q(x_i)(1 + \exp(i\psi) + S(x_i)[1 - \exp(i\psi)]), \tag{42}$$

where

$$S(x_i) = \left(\frac{2}{i}\right)^{1/2} F_\Phi(Z), \qquad Z = \frac{1}{\sigma}\left(\frac{ip}{\pi}\right)^{1/2}\left[x_S - \frac{x_{oi}}{p}\right]. \tag{43}$$

The function $F_\Phi(Z) \approx Z$ for $|Z| < 1$ and $F_\Phi(Z) \approx (i/2)^{1/2}$ for $|Z| > 5$. For typical values of parameters $\gamma r_{ol} \ll F_l$ and $|p - 1| \ll 1$, and the centre of the image appears at the point $x_i^{(c)} = -x_S(r_{il}/r_{ol})$ corresponding the modulo minimum value of the argument Z_c, where $x_S = x_{oi}$. This value can be written as $Z_c = (2/i)^{1/2}(x_S/a_\gamma)$. Assuming that the point of the phase step is located near the XCRL aperture centre (Z_c is less than unity) and replacing $F_\Phi(Z)$ by Z, we obtain

$$I_{\mathrm{i}}(x_{\mathrm{i}}^{(\mathrm{c})}) \approx I_{\mathrm{ib}}(x_{\mathrm{i}}^{(\mathrm{c})}) \left[\cos\left(\frac{\psi}{2}\right) - \frac{2x_{\mathrm{S}}}{a_\gamma} \sin\left(\frac{\psi}{2}\right) \right]^2, \tag{44}$$

where $I_{\mathrm{ib}}(x_{\mathrm{i}})$ is the background intensity, determined by (40). As the point of observation x_{i} moves from the image center $x_{\mathrm{i}}^{(\mathrm{c})}$, the intensity profile approaches the background intensity because $S(x_{\mathrm{i}}) \approx 1$ for x_{i} far from $x_{\mathrm{i}}^{(\mathrm{c})}$. The "phase step" is apparently visible inside the region $|x_{\mathrm{i}} - x_{\mathrm{i}}^{(\mathrm{c})}| < 5\sigma r_{\mathrm{il}}/r_{\mathrm{ol}}$.

It should be noted that the intensity magnitude inside the image region can be reduced (dark image) or enhanced (bright image) compared to the background magnitude. The contrast is different for ψ and $-\psi$, for x_{S} and $-x_{\mathrm{S}}$. However, the simultaneous replacement ψ by $-\psi$ and x_{S} by $-x_{\mathrm{S}}$ remains the image unchanged. The contrast disappears when the object is placed at the position $x_{\mathrm{S}} = -(a_\gamma/2)\tan(\psi/4)$. It is useful to write the analytical solution (44) for the relative intensity in the form

$$\frac{I_{\mathrm{i}}(x_{\mathrm{i}}^{(\mathrm{c})})}{I_{\mathrm{ib}}(x_{\mathrm{i}}^{(\mathrm{c})})} \approx \frac{\cos^2(\psi/2 - \varphi)}{\cos^2(\varphi)}, \quad \tan(\varphi) = -\frac{2x_{\mathrm{S}}}{a_\gamma}. \tag{45}$$

This formula allows us to determine the coordinate of the "phase step" x_{S} for maximum contrast. In the region where $\varphi\psi < \psi^2/4$ the image consists of the intensity pit. In the region where the opposite condition is fulfilled $\varphi\psi > \psi^2/4$ the intensity peak must be observed. The relative height of the peak or the pit increases with increasing the value of $|\varphi - \psi/4|$. We note the formula is valid only for $|\varphi| < 1$.

Let us consider now the transparent object with an arbitrary smooth phase profile $\psi(x_{\mathrm{o}})$ having the finite derivatives $\xi_n(x_{\mathrm{o}}) = \mathrm{d}^n\psi/\mathrm{d}x_{\mathrm{o}}^n$. Since for the given image coordinate x_{i}, the effective region of integration in (5) is $|x_{\mathrm{o}} - x_{\mathrm{oi}}| < \sigma$, we can expand the phase in Taylor's series at the point x_{oi} and restrict ourselves only by the first three terms, namely,

$$\psi(x_{\mathrm{o}}) \approx \psi(x_{\mathrm{oi}}) + \xi_1(x_{\mathrm{oi}})(x_{\mathrm{o}} - x_{\mathrm{oi}}) + \frac{1}{2}\xi_2(x_{\mathrm{oi}})(x_{\mathrm{o}} - x_{\mathrm{oi}})^2. \tag{46}$$

This is correct if the residual terms of the Taylor's series are much less than unity within the interval $|x_{\mathrm{o}} - x_{\mathrm{oi}}| < \sigma$. Using expression (46) for the object wave field $A_{\mathrm{o}}(x_{\mathrm{o}}) = \exp[\mathrm{i}\psi(x_{\mathrm{o}})]$, we calculate the integral (5) as

$$A_{\mathrm{i}}(x_{\mathrm{i}}) \approx \frac{C_0}{\mathrm{i}} \left(\frac{r_{\mathrm{ol}}}{r_{\mathrm{il}} p_{\mathrm{o}}}\right)^{1/2} C_{\mathrm{i}}(x_{\mathrm{i}}) \exp\left(-\frac{\pi}{p_{\mathrm{o}}} \frac{[x_{\mathrm{oi}} + X(x_{\mathrm{oi}})]^2}{a_\gamma^2} \right), \tag{47}$$

where

$$p_{\mathrm{o}} = 1 - \mathrm{i}\gamma\frac{r_{\mathrm{ol}}}{F_{\mathrm{l}}} - \mathrm{i}\xi_2(x_{\mathrm{oi}})\sigma^2, \qquad X(x_{\mathrm{oi}}) = \frac{\lambda r_{\mathrm{ol}}}{2\pi}\xi_1(x_{\mathrm{oi}}). \tag{48}$$

Evidently, if $\xi_1 = \xi_2 = 0$, this expression coincides with (39).

We note that both the second and the first derivatives of the object phase profile influence the image intensity profile. However, the second derivative influences the intensity only slightly if $|\xi_2(x_{\mathrm{oi}})\sigma^2| \ll 1$. On the contrary, the first derivative significantly influences the intensity at the point x_{i}. The reason of this effect cannot be explained within the frame of geometrical optics because it is a consequence of the fact that the imaging provides a finite resolution because the propagator is proportional to the Gaussian instead of the delta-function. Mathematically, even the plane wave leads to the uneven intensity profile (see (39)) due to the integration of the phase factor of the propagator with the linear phase dependence. The additional linear phase profile of the object changes the result of the integration. Under these conditions even a transverse shift of the XCRL will change the image of definite fragment of the object. When $[x_{\mathrm{oi}} + X(x_{\mathrm{oi}})]^2 > x_{\mathrm{oi}}^2$ the intensity decreases compared to the background (dark image). The bright image (increased intensity) can be observed in some places where the opposite condition $[x_{\mathrm{oi}} + X(x_{\mathrm{oi}})]^2 < x_{\mathrm{oi}}^2$ is fulfilled. Of course, when $[x_{\mathrm{oi}} + X(x_{\mathrm{oi}})]^2 = x_{\mathrm{oi}}^2$ the image is determined by the second derivative alone. In the latter case the intensity of X-rays differs slightly from the background value.

The results of this section show that the X-ray compound refractive lens is an excellent device for phase contrast imaging of the transparent objects.

However, the image formed by XCRL is qualitatively different from the image obtained using the in-line phase contrast technique under the near field condition [33]. The latter technique is based on (1), (2) and that $P(x,z)$ is approximately $\delta(x)$ for $z \to 0$. Therefore the difference of $P(x,z)$ from $\delta(x)$ is determined by small distance z. In the case of the XCRL the difference of the propagator $G(x_i, x_o)$ from the delta function is more complicated, namely, it is determined by the finite aperture of the lens due to absorption. Moreover, an additional phase factor becomes essential. A comparison of two techniques for a simple object is made in the next section. Here we note that our results allow one to understand the significant distinction between the images recorded experimentally by the in-line phase contrast technique and with the XCRL (see, for example, [9]).

2.6. Computer simulations

To illustrate the analytical results of 1D imaging presented above, we choose the 1D silicon grid as an object which is homogeneous along the y-axis. The grid has the following parameters: period $p = 20$ μm, bar height $h = 10$ μm, bar width $d = 10$ μm. Usually the grid is located normally to the optical axis (axis z, see Fig. 1) to produce the abrupt phase shift at the boundaries of the bars (see Fig. 2, top profile). However, the grid can be rotated along the y-axis by an angle θ. The rotation changes the phase profile produced by the object. Calculations are made for the experimental setup with the point source of $E = 20$ keV X-ray energy located at the distance $r_s = 50{,}000$ m from the object.

We use standard algorithm of calculation of 1D integral of exponential integrand which consists of replacing the integral by a sum of many fragments Within each fragment the argument of the exponential is approximated by linear function, after that the integral over the fragment is calculated analytically. The short description of the algorithm was done in [34]. We present the normalized intensity as a ratio of the recorded intensity with and without the object.

The very long distance from the source was selected to eliminate some tiny extra oscillations due to the beam divergence. However, it turned out the divergence of the incident beam does not influence the focused images which remain practically the same for $r_s = 50$ m. We note it is not the case for the Fourier images which are dependent of the source distance. The aluminium XCRL has the focal length $F = 1$ m. The refractive index parameters are $\delta = 1.352 \times 10^{-6}$, $\beta = 4.21 \times 10^{-9}$, $\gamma = 3.12 \times 10^{-3}$ for Al and $\delta = 1.21 \times 10^{-6}$, $\beta = 4.72 \times 10^{-9}$ for Si. We take the magnification $M = 1$ and $r_o = r_i = 2$ m. Under these conditions $\sigma = 0.35$ μm.

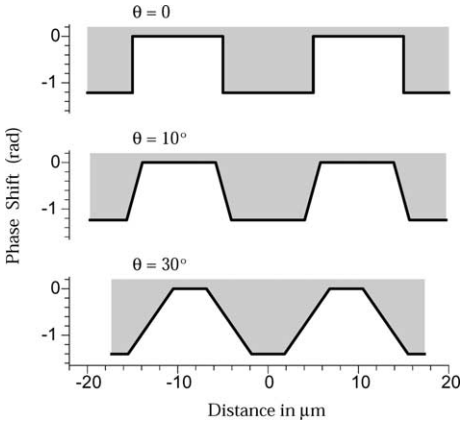

Fig. 2. The central fragments of the phase shift profiles produced by a silicon grid at different angle of rotation θ.

We present calculation results for three values of the rotation angle $\theta = 0°$, 10° and 30°. The fragments of the periodical phase profile produced by the grid are shown in Fig. 2. In the case $\theta = 0$ the phase profile contains a series of positive and negative "phase steps" with $|\psi| = 1.22$, whereas in two other cases the phase profile has regions of constant phase gradient. We calculate both the in-line phase contrast image after the grid and the image produced by the XCRL. For the image without lens we use the formulas (1), (2) with $r_o = 5$ cm, and we convolute the strongly oscillating intensity with the detector line spread function as the Gaussain with FWHM 0.6 μm. In the case of the image with the XCRL the convolution is not necessary.

The results of computer simulations are shown in Figs. 3–5 for $\theta = 0°$, 10° and 30°, respectively. One can see the computer simulations confirm all

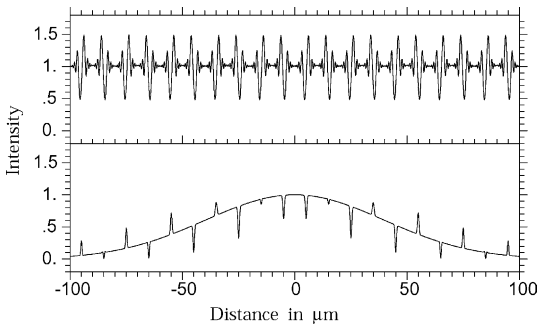

Fig. 3. The normalized intensity distribution (image) for the silicon grid obtained by near field in-line phase contrast technique at 5 cm (top curve) and by XCRL imaging without magnification $M = 1$ (bottom curve) at $\theta = 0$, see text for details.

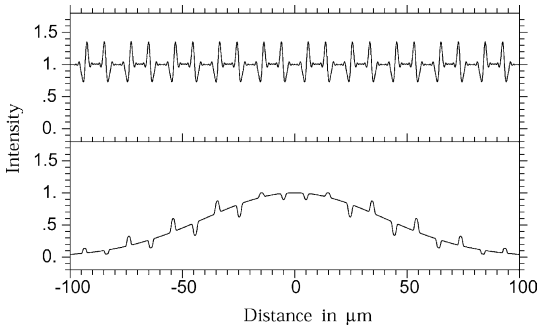

Fig. 4. The same images as in Fig. 3, but at $\theta = 10°$.

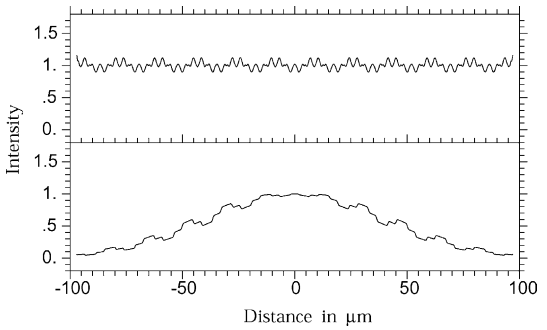

Fig. 5. The same images as in Fig. 3, but at $\theta = 30°$.

the features of the XCRL imaging discussed analytically above (see (45)–(48) and discussion). We note the XCRL image shows always the region with the phase gradient in contrary to the near field phase contrast image. In addition, it is sensitive to the sign of the phase gradient. In the limit case of the ''phase step'' with infinite phase gradient the image is as sharp as possible taking into account the XCRL resolution. We note these properties can lead to the more single-valued and straightforward solution of the phase retrieval problem.

The results of computer simulations for the Fourier-transform of the same Si grid are shown in Fig. 6. In this case $r_i = F$ in a thin lens approximation whereas $r_o = 0$ to obtain the better image, as it follows from the analytical consideration. The figure shows the decimal logarithm of the relative intensity because the intensity decreases sharply for the image periphery. The top figure shows many diffraction orders of the periodical grid. The all even orders, except zero, are absent due to the structure factor of the grid. All peaks are shown sharply despite the significant difference in value. So the periphery peaks are in 10^{-4} times smaller than the zero-order peak. The figure at $\theta = 10°$ does not contain high order peaks, and the even orders become visible. The figure at $\theta = 30°$ shows no difference between the even and odd orders peaks. The high order peaks are sharply decreased. We note all peaks are present but they are very weak.

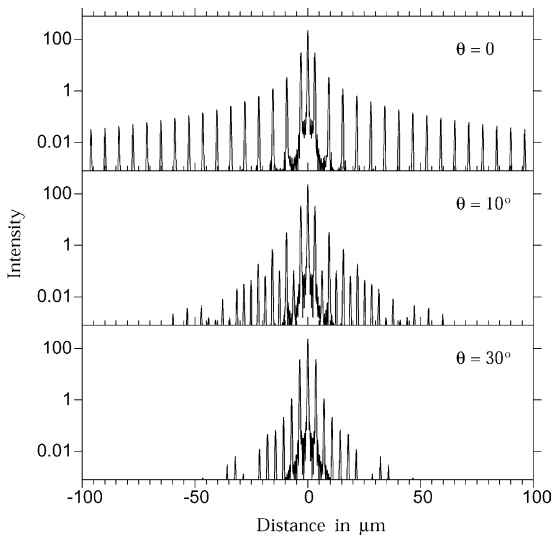

Fig. 6. The distribution of the normalized intensity (Fourier transform) calculated for the distance equal to the XCRL focal length. The silicon grid is placed in front of the XCRL. Different values of the rotation angle θ are pointed at the curves.

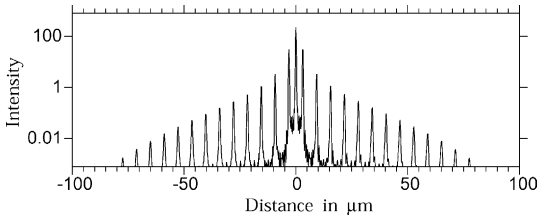

Fig. 7. The distribution of the normalized intensity (Fourier transform) calculated for the distance equal to the XCRL focal length. The silicon grid is placed at 2 m before the XCRL. The rotation angle $\theta = 0$.

As follows from the theory, the Fourier transformation becomes conditional with increasing the distance r_o. Fig. 7 shows the results of computer simulation for the grid at $\theta = 0$ and $r_o = 2$ m. The higher orders become damped while the principal orders remain practically unchanged.

3. The diffraction theory of the 2-D imaging with parabolic X-ray compound refractive lenses

In this section we show that the wave field distributions along the x-axis and y-axis propagate independently of each other within the paraxial approximation.

First of all, the free-space 2-D propagator is equal to

$$P^{(2)}(x,y,z) = P^{(1)}(x,z)P^{(1)}(y,z), \tag{49}$$

where $P^{(1)}(s,z)$ is determined by (2). Hereafter s is any one of the coordinate x and y. For the parabolic XCRL with round aperture the variable thickness along the optical axis is equal to

$$t(x,y) = N\left[\frac{x^2+y^2}{R} + d\right], \quad (x^2+y^2) < \frac{D^2}{4}, \quad L = t\left(\frac{D}{2},0\right), \tag{50}$$

where D is a diameter of the XCRL aperture.

In the thin lens approximation the XCRL 2-D propagator can be written as a product of the 1-D propagators

$$P_1^{(2)}(x_b,x_f,y_b,y_f) = P_1^{(1)}(x_b,x_f)P_1^{(1)}(y_b,y_f), \tag{51}$$

where

$$P_1^{(1)}(s_b,s_f) = \exp\left(-ikc\delta\frac{d}{2}N - ikc\frac{s_b^2}{2F}\right)\delta(s_b - s_f). \tag{52}$$

We note without a derivation that the XCRL 2-D propagator has the same property in the linear approximation in L/F considered above.

This allows us to calculate the integrals on x and y variables independently. The calculations are completely the same as presented above. Then the image 2-D propagator is a product of two 1-D propagators

$$G^{(2)}(x_i,x_o;y_i,y_o) = G^{(1)}(x_i,x_o)G^{(1)}(y_i,y_o). \tag{53}$$

Here $G^{(1)}(x_i,x_o)$ is determined by (24) and (25) with replacing d by $d/2$. The general image problem can be formulated as

$$A_i(x_i,y_i) = \int dx_o\,dy_o G^{(2)}(x_i,x_o;y_i,y_o)A_o(x_o,y_o). \tag{54}$$

In general case of an arbitrary object the two-dimensional integral must be calculated and further simplification is impossible.

However, in special cases, when the object wave field is factorisable, i.e., $A_o(x_o,y_o) = P_o(x_o)Q_o(y_o)$, the image wave field is factorisable too, $A_i(x_i,y_i) = P_i(x_i)Q_i(y_i)$, and the relation between the object wave field and the image wave field can be calculated for each axis independently. This takes place, for example, for the homogeneous object illuminated by the spherical wave in the paraxial approximation and for one- or two-dimensional grid. It is worthwhile to note if the lens formula is fulfilled, the propagator is strongly localized. In this case it is sufficient to have approximately local factorisation of the wave field.

4. Conclusion

We develop the diffraction theory for the formation of the image with parabolic X-ray compound refractive lenses in the paraxial approximation. We obtain the analytical expression for the image propagator which allows us to explain the imaging and focusing properties of the

XCRL. We develop the enhanced thin lens approximation for the relatively long XCRL with the longitudinal size L taking into account the linear in L/F corrections. We show that the focal length for the long XCRL is $F + L/6$ when it is measured from its center, where $F = R/2N\delta$ is the focal length in the thin lens approximation.

The relatively small effective aperture of the XCRL due to the absorption of X-rays on all materials results in the finite resolution of the image propagator. This leads to developing phase or edge enhanced imaging effects, which make visible transparent objects at the image distance which satisfy the lens formula. We found out that these edge enhanced images are associated with the local phase gradient of the X-ray wave field modified by the object. Moreover, these images are sensitive to the sign of the phase gradient. Thus the XCRL-based imaging is different from the conventional in-line phase contrast technique [33]. It opens a new possibility for micro-imaging of the non-absorbing objects.

We study the optical properties of the XCRL as a Fourier transformer and show that the Fourier transformation made by the XCRL at the focal plane becomes conditional due to the finite XCRL aperture. We obtain that the XCRL always shows the Fourier transformation of the wave field formed in front of the lens and modified by the lens aperture. When the object is placed at the remote distance from the XCRL the subsequent propagation of the radiation through the free space yields a significant modification of the wave field.

The computer simulations allow us to confirm the analytical formulas. We obtain that the two-dimensional image propagator is a product of one-dimensional image propagators for x-axis and y-axis. This can simplify the calculation of the images for many objects which structure can be described by a product of two functions, each of them represents the separate coordinate axis.

References

[1] A. Snigirev, V. Kohn, I. Snigireva, B. Lengeler, Nature 384 (1996) 49.

[2] A. Snigirev, B. Filseth, P. Elleaume, Th. Klocke, V. Kohn, B. Lengeler, I. Snigireva, A. Souvorov, J. Tummler, SPIE Proc. 3151 (1997) 164.

[3] A. Snigirev, V. Kohn, I. Snigireva, A. Souvorov, B. Lengeler, Appl. Opt. 37 (1998) 653.

[4] P. Elleaume, J. Synchr. Radiat. 5 (1998) 1.

[5] B. Lengeler, J. Tummler, A. Snigirev, I. Snigireva, C. Raven, J. Appl. Phys. 84 (1998) 5855.

[6] B. Lengeler, C.G. Schroer, M. Richwin, J. Tummler, M. Drakopoulos, A. Snigirev, I. Snigireva, Appl. Phys. Lett. 74 (1999) 3924.

[7] A.Q.R. Baron, Y. Kohmura, V.V. Krishnamurty, Yu.V. Shvydko, T. Ishikawa, J. Synchr. Radiat. 6 (1999) 953.

[8] B. Lengeler, C. Schroer, J. Tummler, B. Benner, M. Richwin, A. Snigirev, I. Snigireva, M. Drakopoulos, J. Synchr. Radiat. 6 (1999) 1153.

[9] C.G. Schroer, B. Lengeler, B. Benner, M. Kuhlmann, T.F. Gunzler, J. Tummler, C. Rau, T. Weitkamp, A. Snigirev, I. Snigireva, SPIE Proc. 4145 (2001) 274.

[10] V. Aristov, M. Grigoriev, S. Kuznetsov, L. Shabelnikov, V. Yunkin, T. Weitkamp, C. Rau, I. Snigireva, A. Snigirev, M. Hoffmann, E. Voges, Appl. Phys. Lett. 77 (2000) 4058.

[11] V.V. Aristov, M.V. Grigoriev, S.M. Kuznetsov, L.G. Shabelnikov, V.A. Yunkin, M. Hoffmann, E. Voges, Opt. Commun. 177 (2000) 33.

[12] V. Aristov, M. Grigoriev, S. Kuznetsov, L. Shabelnikov, V. Yunkin, C. Rau, A. Snigirev, I. Snigireva, T. Weitkamp, M. Hoffmann, E. Voges, SPIE Proc. 4145 (2001) 285.

[13] A.Q.R. Baron, Y. Kohmura, Y. Ohishi, T. Ishikawa, Appl. Phys. Lett. 74 (1999) 1492.

[14] J.T. Cremer, M.A. Piestrup, H.R. Beguiristain, C.K. Gary, R.H. Pantell, R.H. Tatchyan, Rev. Sci. Instr. 70 (1999) 3545.

[15] M.A. Piestrup, J.T. Cremer, H.R. Beguiristain, C.K. Gary, R.H. Pantell, Rev. Sci. Instr. 71 (2000) 4375.

[16] H.R. Beguiristain, J.T. Cremer, M.A. Piestrup, R.H. Pantell, C.K. Gary, J. Feinstein, SPIE Proc. 4144 (2000) 155.

[17] M.A. Piestrup, H.R. Beguiristain, C.K. Gary, J.T. Clemer, R.H. Pantell, R. Tatchyn, Nucl. Instr. Meth. B 173 (2001) 170.

[18] Y. Ohishi, A.Q.R. Baron, M. Ishii, T. Ishikawa, O. Shimomura, Nucl. Instr. Meth. A 467–468 (2001) 962.

[19] Yu.I. Dudchik, N.N. Kolchevskii, Nucl. Instr. Meth. A 421 (1999) 361.

[20] Y. Kohmura, M. Awaji, Y. Suzuki, T. Ishikawa, Yu.I. Dudchik, N.N. Kolchevsky, F.F. Komarov, Rev. Sci. Instr. 70 (1999) 4161.

[21] Yu.I. Dudchik, N.N. Kolchevsky, F.F. Komarov, Y. Kohmura, M. Awaji, Y. Suzuki, T. Ishikawa, Nucl. Instr. Meth. A 454 (2000) 512.

[22] Yu.I. Dudchik, N.N. Kolchevsky, SPIE Proc. 4145 (2001) 235.

[23] B. Cederstrom, R. Cahn, M. Danielsson, M. Lundqvist, D.R. Nygren, Nature 404 (2000) 951.

[24] B. Cederstrom, M. Danielsson, M. Lundqvist, SPIE Proc. 4145 (2001) 294.

[25] V.V. Protopopov, K.A. Valiev, Opt. Commun. 151 (1998) 297.

[26] V.V. Protopopov, Opt. Commun. 172 (1999) 113.

[27] R.H. Pantell, J. Feinstein, H.R. Beguiristain, M.A. Piestrup, C.K. Gary, J.T. Cremer, Rev. Sci. Instr. 72 (2001) 48–52.
[28] C.G. Schroer, B. Benner, T.F. Gunzler, M. Kuhlmann, B. Lengeler, C. Rau, T. Weitkamp, A. Snigirev, I. Snigireva, in: Ulrich Bonse (Ed.), Developments in X-ray Tomography III, Proc. of SPIE 4503, 2002, p. 23–33.
[29] T. Weitkamp, C. Rau, A. Snigirev, in: Ulrich Bonse (Ed.), Developments in X-ray Tomography III, Proc. of SPIE 4503, 2002, p. 92–102.
[30] M. Born, E. Wolf, Principles of Optics, seventh ed., Cambridge University Press, Cambridge, 1999.
[31] V.G. Kohn, Phys. Scr. 56 (1997) 14.
[32] J.-P. Girardeau-Montaut, C. Girardeau-Montaut, Opt. Commun. 198 (2001) 1.
[33] A. Snigirev, I. Snigireva, V. Kohn, S. Kuznetsov, I. Schelokov, Rev. Sci. Instr. 66 (1995) 5486.
[34] V.G. Kohn, I. Snigireva, A. Snigirev, Phys. Stat. Sol. (b) 222 (2000) 407.